Steam Reforming of Methane and Water-Gas Shift in Catalytic Wall Reactors

K. Venkataraman, E. C. Wanat, and L. D. Schmidt
Dept. of Chemical Engineering and Materials Science, University of Minnesota, Minneapolis MN 55455

Catalytic wall reactors permit high heat-transfer rates between exothermic and endothermic reactions taking place catalytically on opposite sides of a thin wall, because they eliminate resistance to heat transfer in thermal boundary layers, thus making them compact and efficient. A parallel plate catalytic wall reactor was built in which exothermic methane combustion on platinum and endothermic methane steam reforming on rhodium occurred on walls in alternate channels. This reactor gave 95% conversion of methane to synthesis gas with a residence time of ~70 ms at a steam/methane ratio of 1/1 with a thermal efficiency of ~60%. A preheat pass was added on the combustion side that enabled heat exchange between hot combustion products and cold combustion inlet gases to increase temperature upstream and decrease it downstream. This two-pass reactor gave H_2/CO ratios of ~14/1 with a residence time of ~170 ms at a steam/methane ratio of 4/1. To increase the H_2/CO ratio, the endothermic channel length was also extended, with a platinum-ceria wall coating on the extended region to further reduce downstream temperatures and promote water-gas shift. This reactor gave downstream temperatures as low as 200°C, and produced H_2/CO ratios as high as 42/1 with a residence time of ~300 ms at a steam/methane ratio of 4/1. The extended reactor shows good potential for producing high H_2/CO ratio product streams suitable for preferential oxidation and subsequent use in fuel cells in a scalable configuration.

Introduction

Steam reforming of hydrocarbons requires temperatures of 800 to 900°C for high equilibrium yields. It is typically carried out in tubes packed with catalyst coated pellets with burners operating at ~1,500°C outside the tubes to provide heat for the endothermic reactions. The high heat-transfer resistance between the flames and the catalyst pellets necessitates high flame temperatures and results in reformer residence times of several seconds.

The catalytic wall reactor consists of a thin wall coated with the same or different catalysts on the two sides (Frauhammer et al., 1999; Polman et al., 1999; Zalc and Löffler, 2002). An exothermic reaction (such as combustion) takes place on one side, which provides heat for an endothermic reaction occurring on the other side. Carrying out reactions on two sides of a thin wall eliminates heat-transfer resistance in thermal boundary layers, thus increasing heat-transfer rates and reducing residence times. Conventional reactor sizes can be reduced by a comparable factor (typically by a factor of at least 10) if residence times can be reduced from a few seconds to a few milliseconds. Catalytic wall reactors in parallel plate configurations can also be scaled more easily than multitube reactors in furnaces. Another advantage of catalytic wall reactors is the lower operating temperatures in catalytic combustion as compared to flame combustion, thus eliminating NO_x formation.

Catalytic wall reactors have been examined for several years. Koga and Watanabe (1991) described a plate type reformer that coupled catalytic combustion and reforming, which took place in alternate channels. The catalysts filled the gaps between the plates and were not deposited on the

Correspondence concerning this article should be addressed to L. D. Schmidt.

walls, which resulted in higher heat-transfer resistance. Igarashi et al. (1992) described a wall reactor that used a heating medium to supply heat for an endothermic reaction that occurred on walls in alternate channels, although the presence of a thermal boundary layer in the combustion channel resulted in high heat-transfer resistance. Frauhammer et al. (1999) described a reactor that coupled catalytic combustion and methane steam reforming in alternate channels with catalysts coated on both sides of the walls. They carried out preliminary experiments using a ceramic honeycomb monolith with specially designed distribution channels for the combustion and process gases. Polman et al., (1999) described and tested a metal flat plate reactor for same reaction system. Both of these systems were operated successfully only below ~ 800°C, and the stability of catalyst and wall materials, and heat losses from the reactor, seemed to limit successful operation in these systems. Zalc and Löffler (2002) described a plate reformer for methane steam reforming that consisted of a single reforming channel with a combustion channel on either side. Temperatures and residence times were not discussed for most of these systems. Water-gas shift reactions to increase H_2/CO ratios were not considered in any of these systems.

Redenius et al. (2001) described a radiant burner that consisted of catalyst coated on one side of a thin metal wall. Methane combustion on platinum generated the radiant energy, and multiple passes were added to recuperate energy from the hot combustion products. The burner was operated at temperatures ~ 950 to 1,200 K with a radiant efficiency of $\sim 60\%$.

Venkataraman et al. (2002) described a coupled catalytic wall reactor in a concentric tube configuration using quartz tubes that operated at temperatures $\sim 1{,}000$°C and enabled efficient heat exchange between methane catalytic combustion and homogeneous ethane cracking. High ethane conversions and ethylene selectivities (77% and 87%, respectively) were obtained at contact times of ~ 50 ms. Temperature profiles for systems with multiple passes on the combustion side, and for co-current and counter-current modes of operation, were measured.

In this research, the results from the concentric tube configuration are extended to a parallel plate configuration with catalysts coated on both sides of the plates, and the performance of the parallel plate reactor for syngas (a mixture of CO and H_2) and hydrogen production is evaluated.

Reactions

We consider the coupling of the catalytic combustion of methane on platinum

$$CH_4 + 2O_2 \rightarrow CO_2 + 2H_2O, \quad \Delta H_{298} = -802.6 \text{ kJ/mol}$$

with the steam reforming of methane on rhodium

$$CH_4 + H_2O \rightarrow CO + 3H_2, \quad \Delta H_{298} = +205.6 \text{ kJ/mol}$$

Water-gas shift on rhodium or platinum-ceria may also take place in the endothermic reaction channels by the reaction

$$CO + H_2O \leftrightarrow CO_2 + H_2, \quad \Delta H_{298} = -41.0 \text{ kJ/mol}$$

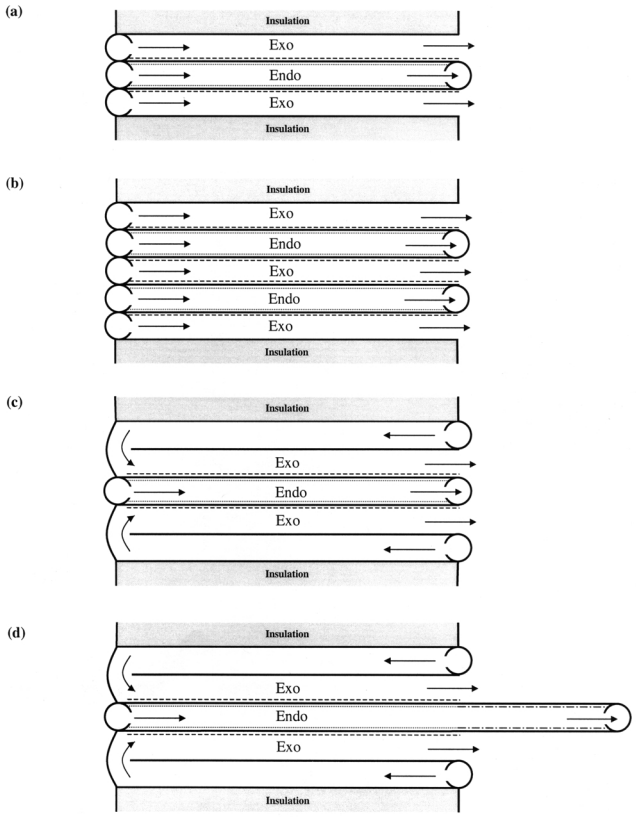

Figure 1. One- and two-pass cocurrent systems.

"Exo" and "Endo" denote exothermic and endothermic reactions occurring on catalyst coated walls, respectively. Arrows indicate directions of flow. (a) One-pass three-channel system; (b) one-pass, five-channel system; (c) Two-pass, three-channel system; (d) extended two-pass 3-channel system.

From the heats of reaction of combustion and reforming, it is seen that combusting 1 mole of CH_4 releases enough heat to reform approximately 4 moles of CH_4. However, heat losses in the reactor and sensible heat absorption by reactants and products decrease the number of moles of CH_4 that can be reformed per mole of CH_4 combusted.

Experimental System

Figure 1 shows various parallel plate configurations that could be used for coupling exothermic and endothermic reactions, with arrows indicating directions of flow. Figure 1a depicts a one-pass, three-channel system with two exothermic channels and one endothermic channel. The exothermic and endothermic flows in these alternate channels are cocurrent, but these systems can be run in the countercurrent mode as well. The one-pass five-channel configuration in Figure 1b is similar to that in Figure 1a, but it has 3 exothermic and 2 endothermic channels, suggesting that these systems can be scaled up simply by adding more channels. The two-pass three-channel configuration in Figure 1c allows heat exchange between the hot exothermic products and cold exothermic reactants, which results in a sharp axial temperature gradient. The extended two-pass three-channel configuration in Figure 1d extends the length of only the endother-

mic channel of the two-pass system to further decrease downstream temperatures.

In this research, we present results mainly from experiments conducted using the configurations depicted in Figures 1a, 1c, and 1d.

Reactor structure

The reactor was in a parallel plate configuration, as sketched in Figures 1a–1d. The plates were 8 cm × 5 cm × 0.1 mm corrugated fecralloy (a 73% Fe, 20% Cr, 5% Al and < 1% Ni + Si alloy) sheets with corrugations perpendicular to the direction of flow. For the extended two-pass reactor, the catalyst coated plates were 13 cm long. The reactants entered the reactor through 5 equally spaced 0.5 mm holes across the 5 cm width. The product gases on the endothermic side exited through a 1 mm wide slot into a collection tube. The gaps between the plates were nominally 4 mm in all the configurations shown in Figure 1. Fiberfrax paper was used as a gasket between the plates and the stainless steel frames that held the plates, and the frames were tightly bolted on the outside.

Fecralloy has a melting point of ~1,500°C, making it suitable for use in the coupled catalytic wall reactor. We used this reactor up to >1,200°C with no visible deterioration in the alloy. The plates used in the reactor have 1 mm deep corrugations that make them more rigid and prevent warping, which helps maintain a uniform gap between the plates. The corrugations also increase surface area over flat plates, and promote gas mixing and better heat transfer between the gases and the wall.

Catalyst preparation

The fecralloy plates were first oxidized in air in an oven at 900°C for ~5 h, thus forming a layer of alumina on the surface that improved adhesion of the washcoat and catalyst. The surfaces were then coated with an alumina washcoat and a catalyst in a manner similar to that described by Venkataraman et al. (2002).

The washcoat was an aqueous suspension of ~10 wt% γ-alumina powder having 3 μm particles, and contained 1 wt. % Cr_2O_3 from $Cr(NO_3)_3$ and 0.1 wt. % Y_2O_3 from $Y(NO_3)_{3.6}H_2O$ (Redenius et. al., 2001). One of two coatings of the washcoat were applied to produce a coating ~10 μm thick. The γ-alumina was partially converted to α-alumina, which has a less porous structure, when the washcoat was briefly fired to ~1,000°C during preparation. The washcoat adhered well to the fecralloy, and did not flake off even after many hours of operation.

Platinum (from 8 wt. % H_2PtCl_6 solution) and rhodium (from 13.9 wt. % $Rh(NO_3)_3$ solution) were used as the combustion and reforming catalysts, respectively. The extended region in the extended two-pass reactor was coated with platinum-ceria, a 1:1 by volume mixture of 5 wt. % $Ce(NO_3)_3$ solution and 8 wt. % H_2PtCl_6 solution, to promote water-gas shift reactions. A fecralloy plate coated with rhodium on both sides was also placed in the endothermic channel in the one- and two-pass reactors, and a similar plate coated with platinum-ceria was placed in the extended region of extended two-pass reactor. These plates increased catalytic surface area, while maintaining uniform temperatures.

Apparatus

Compressed air, methane, and nitrogen at room temperature were delivered from cylinders and metered by mass-flow controllers. Nitrogen was used as a reference gas for gas chromatographic analysis of the product gases from the endothermic and exothermic sides. Water from a pressurized tank was delivered by an automotive fuel injector to a heated quartz tube that generated steam for the endothermic channel. An electronic pulse generator connected to the fuel injector controlled the steam flow rate. Metal tubes with equal restrictions were used to deliver the reactants to the reactor inlets to ensure equal flow rates in all the exothermic or endothermic channels. The exothermic and endothermic gases entered these tubes at 25°C and 300°C, respectively.

Startup

After the methane and air flows were started, the exothermic reaction was ignited by heating the reactor with a Bunsen burner to a temperature (~600°C) at which ignition on platinum takes place. Ignition of all platinum surfaces was achieved in ~30 s for the one-pass system and in ~60 s for the two-pass system. After ignition of the platinum surfaces in all the channels, the Bunsen burner was removed, and nitrogen, steam, and methane flows to the endothermic channels were started. All gas flows are reported as standard liters per minute (slpm) at 1 atm and 273 K, and steam flows on the endothermic side are reported as steam/CH_4 (S/C) molar ratios. The flow rates reported here are the sum totals of flows in all the exothermic or endothermic channels. All residence times were corrected for gas temperature and volumetric flow rate changes due to reaction. These were estimated as the channel volume divided by the endothermic gases volumetric flow rate based on an average channel temperature. Nominal residence times quoted are estimated to be accurate to within ±10%.

Measurements

Temperatures were measured in the exothermic channel (Figure 2) with a 0.16 cm inconel sheathed chromel-alumel thermocouple. Upstream temperatures were measured 1 cm downstream of the inlet in the exothermic channel, and downstream temperatures were measured at the position of the endothermic product gas exit in the exothermic channel. Temperatures are regarded as accurate to ±50°C and positions to ±0.5 cm. Fairly uniform flows of the reactants across the width of the channel were obtained, as seen from the centerline and edge temperature profiles obtained in an exothermic channel of a two-pass system, as shown in Figure 2. The temperature difference between the centerline and the edge at any position along the flow direction was <100°C for all reactor configurations.

Gases were analyzed by gas chromatography using samples withdrawn by a syringe from exothermic or endothermic effluents. Measurements were accurate to ±5%, and carbon balances closed to ±7%. CH_4 conversions and CO selectivities are regarded as accurate to ±1%.

CH_4 concentrations on the exothermic side were varied from 6.4% (lean) to 9.5% (stoichiometric) CH_4 in air. Exothermic CH_4 conversions ~90% or greater were ob-

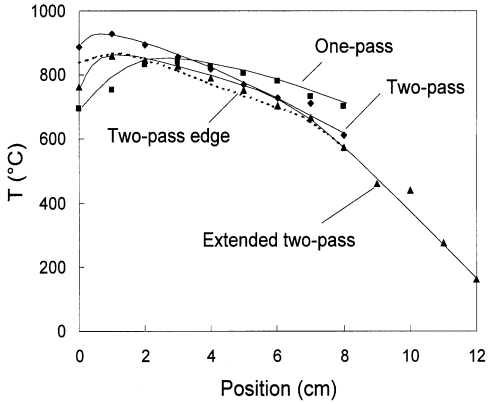

Figure 2. Measured centerline temperature profiles in the one-, two- and extended two-pass, three-channel co-current systems.

All temperatures were measured in the exothermic channels. The flow rates of the exothermic gases were 0.3 slpm CH_4 and 3 slpm air. The flow rates of the endothermic gases were 0.2 slpm CH_4 and 0.2 slpm N_2 with a S/C ratio of 3/1. The dashed curve indicates the measured temperature near the edge, showing that the temperature difference from center to edge is $< 100°C$

tained for all these systems. The adiabatic efficiency of all these systems was estimated to be ~ 55 to 60%.

Results

The performances of the various reactors shown in Figure 1 are presented in this section. We show that the temperature profile in the one-pass co-current system is suitable for methane steam reforming, resulting in products with H_2/CO ratios of $\sim 3/1$, whereas the temperature profiles in the two-pass and extended two-pass co-current systems are suitable for both methane steam reforming and water-gas shift, resulting in products with H_2/CO ratios $\gg 3/1$.

$H_2 + CO$ in a one-pass system

Figure 2 shows a measured centerline temperature profile in a one-pass, three-channel cocurrent system depicted in Figure 1a. It is seen that the temperature was almost constant along the length of the channel, which is similar to the temperature profile observed for the concentric tube configuration by Venkataraman et. al. (2002). The CH_4 conversion, CO selectivity, and H_2/CO ratios in the endothermic product stream as a function of the endothermic CH_4 flow at a S/C ratio of 1/1 and fixed exothermic CH_4 flow are shown in Figure 3a. CO selectivities increased and CH_4 conversions decreased with increasing CH_4 flows. Figure 3b shows the trade-off between residence time and CO selectivity. Lower residence times (higher endothermic CH_4 flows) resulted in higher CO selectivities because not much water-gas shift, which has slower kinetics than steam reforming, took place. Although it seems paradoxical that reduced downstream temperatures led to less water-gas shift (an exothermic reaction), it should be noted that the lower temperatures in this case were due to higher endothermic CH_4 flows, which resulted in lower residence times. For endothermic flows of 0.7 slpm CH_4 and 0.2 slpm N_2 at a S/C ratio of 1/1 and exothermic

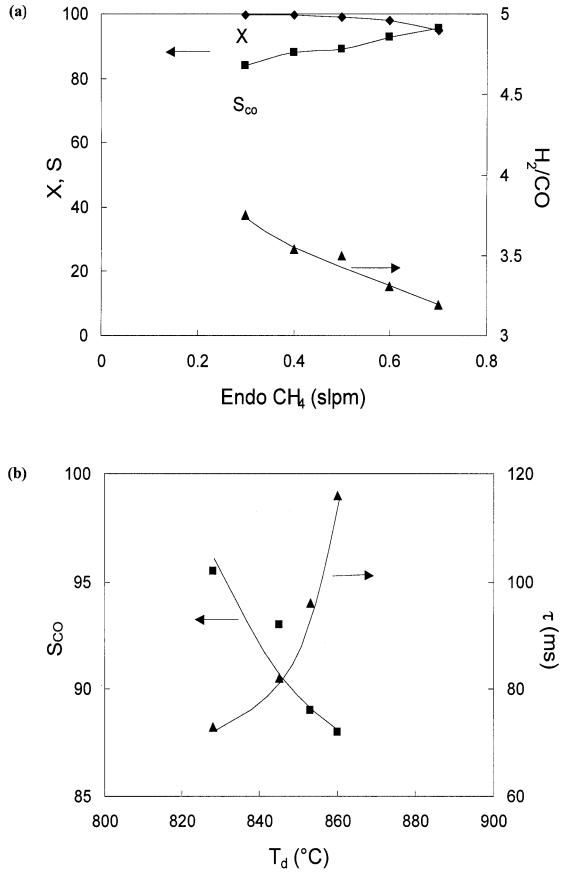

Figure 3. Measured results of the one-pass system.

(a) Endothermic CH_4 conversion (X), CO selectivity (S_{CO}), and H_2/CO ratio as a function of the endothermic CH_4 flow rate in a one-pass, three-channel system. The endothermic N_2 flow rate was 0.2 slpm with a S/C ratio of 1/1. The flow rates of the exothermic gases were 0.63 slpm CH_4 and 6 slpm air. (b) Measured CO selectivity (S_{CO}) and residence time (τ) as a function of downstream temperature (T_d) in a one-pass 3-channel system at the conditions above.

flows of 0.63 slpm CH_4 and 6 slpm air, we obtained $\sim 95\%$ endothermic CH_4 conversion, $\sim 95\%$ CO selectivity, and a H_2/CO ratio of $\sim 3/1$ at a residence time of ~ 70 ms.

A one-pass, five-channel cocurrent system depicted in Figure 1b was also built and tested. This system was not studied as extensively as the three-channel systems. Endothermic CH_4 conversions $> 90\%$ were obtained for various exothermic and endothermic flows.

$H_2 + CO$ in a two-pass system

Figure 2 shows a measured centerline temperature profile in a two-pass, three-channel cocurrent system depicted in Figure 1c. The temperature was highest in the upstream section and fell rapidly in the downstream section, which is consistent with the temperature profile for the concentric tube configuration reported by Venkataraman et al. (2002). The high upstream and the lower downstream temperatures are favorable for endothermic steam reforming and exothermic water-gas shift, respectively. Since low downstream tempera-

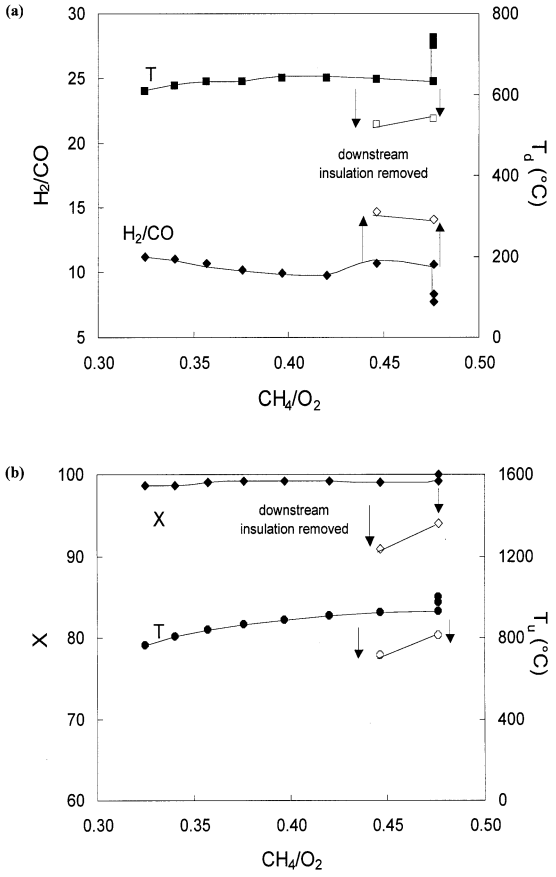

Figure 4. Measured results of the two-pass system.

(a) Downstream temperature (T_d) and H_2/CO ratio as a function of CH_4/O_2 ratio of the combustion gases in a two-pass, 3-channel system. The exothermic CH_4 flow rates were 0.5, 0.4, and 0.3 slpm. The flow rates of the endothermic gases were 0.2 slpm CH_4 and 0.2 slpm N_2 with a S/C ratio of 4/1. The effect of removing downstream insulation is also illustrated by open symbols. (b) Upstream temperature (T_u) and endothermic CH_4 conversion (X) as a function of CH_4/O_2 ratio of the combustion gases in a two-pass, three-channel system at the conditions above.

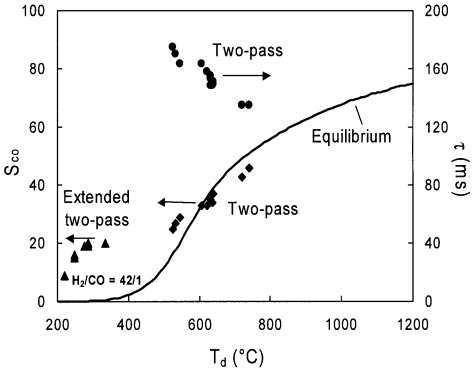

Figure 5. Comparing the two-pass and extended two-pass systems.

Measured CO selectivity (S_{CO}) and residence time (τ) as a function of downstream temperature (T_d) in a two-pass, three-channel system and an extended two-pass, three-channel system at a S/C ratio of 4/1. The solid curve represents calculated equilibrium CO selectivity for a starting mixture of CH_4 and steam at a S/C ratio of 4/1 as a function of temperature.

tures were possible, experiments were conducted to see how low of a downstream temperature could be achieved.

Figure 4 shows the effect of first decreasing the exothermic CH_4 flow at a fixed CH_4/air ratio (closed symbols; top to bottom for temperatures and conversion, bottom to top for H_2/CO) and then increasing the air flow at a fixed exothermic CH_4 flow (closed symbols; right to left). The upstream and downstream temperatures dropped sharply as the exothermic CH_4 flow was decreased, and then slightly as the air flow was increased. The endothermic CH_4 conversion followed a trend similar to the upstream temperature as shown in Figure 4b, and the H_2/CO ratio increased with decreasing downstream temperatures (Figure 4a) due to more water-gas shift. Removing insulation from the downstream section of the reactor (open symbols; arrows) resulted in lower upstream and downstream temperatures, which also led to lower endothermic CH_4 conversions and higher H_2/CO ratios.

Figure 5 shows residence time and CO selectivity as a function of the downstream (exit) temperature. CO selectivities decrease with increasing residence times and lower downstream temperatures, because more water-gas shift occurs in the downstream section. The CO selectivities match those predicted by equilibrium at the operating S/C ratio of 4/1. For endothermic flows of 0.2 slpm CH_4 and 0.2 slpm N_2 at a S/C ratio of 4/1 and exothermic flows of 0.3 slpm CH_4 and 3 slpm air, we obtained $\sim$94% endothermic CH_4 conversion, $\sim$27% CO selectivity, and a H_2/CO ratio of $\sim$14/1 at a residence time of $\sim$170 ms.

High H_2/CO ratios in an extended two-pass system

The exit gas composition in the two-pass system (Figure 5) was near equilibrium at the exit temperature, so a further reduction in temperature would be required to further increase H_2/CO ratios. This was achieved in the extended two-pass configuration. Experiments in our laboratory have shown that rhodium is not very active for water-gas shift at short contact times at temperatures below 600°C (Wheeler and Schmidt, 2002), so we used a platinum-ceria catalyst (Trovarelli, 2002), which was coated on the walls in the extended region. Figure 2 shows a measured centerline temperature profile in an extended two-pass 3-channel co-current system depicted in Figure 1d. The extended region was not insulated to decrease temperature more rapidly. The high upstream temperatures and low downstream temperatures are similar to the two-pass temperature profile, but the temperature fell sharply in the extended section, which is favorable for the exothermic water-gas shift reaction. Figure 5 shows CO selectivity as a function of the downstream temperature. The CO selectivities are 10 to 20% higher than those predicted by equilibrium at the exit temperature at the operating S/C ratio of 4/1.

Figure 6 shows CO selectivities and H_2/CO ratios at various endothermic CH_4 flows and S/C ratios as a function of the residence time. The CO selectivity increased and the H_2/CO ratio decreased with increasing endothermic CH_4 flows that resulted in lower residence times. Lower CO selectivities and higher H_2/CO ratios were observed at higher S/C

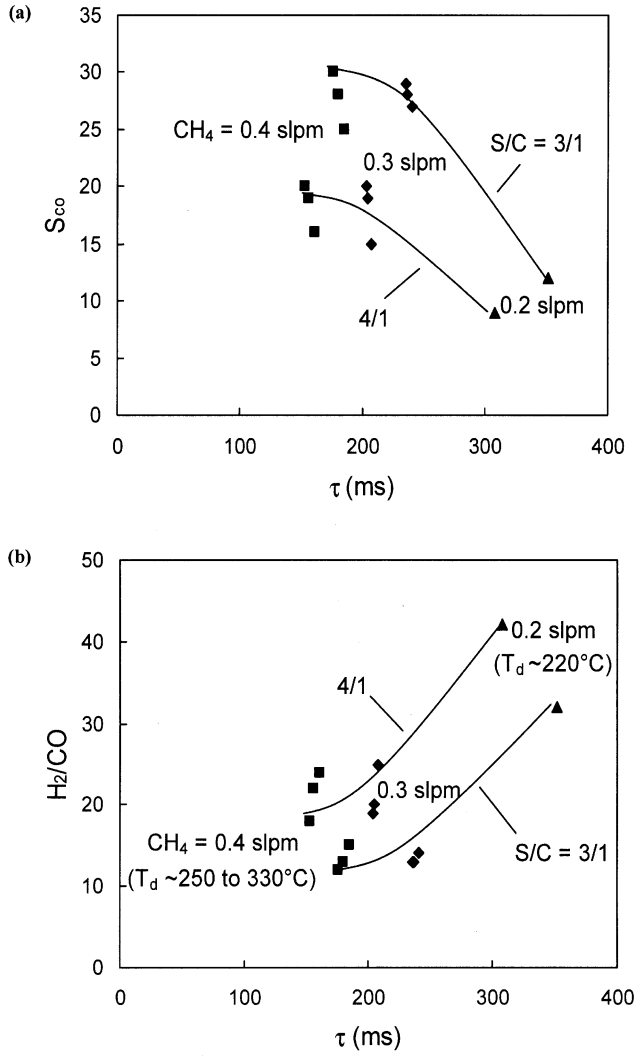

Figure 6. Measured results of the extended two-pass system.

(a) Measured CO selectivity (S_{CO}) as a function of residence time (τ) in an extended two-pass, three-channel system. The flow rates of the endothermic gases were 0.2, 0.3, and 0.4 slpm CH_4 and 0.2 slpm N_2, with S/C ratios of 3/1 and 4/1. The flow rates of the exothermic gases were 0.3, 0.4, and 0.5 slpm CH_4 at constant CH_4/air ratios of 1/10. (b) H_2/CO ratio as a function of residence time (τ) in an extended two-pass 3-channel system at the conditions above. T_d denotes downstream exit temperatures measured in the extended region on the exothermic side wall.

ratios as expected. For endothermic flows of 0.2 slpm CH_4 and 0.2 slpm N_2 at a S/C ratio of 4/1 and exothermic flows of 0.3 slpm CH_4 and 3 slpm air, we obtained $\sim$92% endothermic CH_4 conversion, $\sim$9% CO selectivity, and a H_2/CO ratio of $\sim$42/1 at a residence time of $\sim$300 ms.

Simulation

Heat transfer between the reaction streams, CH_4 conversions, and product selectivities for most systems discussed here were simulated using the CFD-ACE software package, which can handle chemically reacting flows in user-defined geometries. Methane combustion on platinum was simulated using the mechanism of Deutschmann et al. (2000), which has 10 species and 24 reactions, and methane steam reforming and water-gas shift on rhodium were simulated using the mechanism of Klein and Schmidt (2002) which has 12 species and 42 reactions. No gas-sphase reactions were considered because previous results (Redenius et. al., 2001) suggest they are not important for these conditions.

Features

In these simulations, the full two-dimensional (2-D) Navier-Stokes and energy conservation equations were solved to determine the composition, flow, and temperature fields. These simulations incorporated the following features:

- Radiation heat exchange between surfaces. Surfaces and boundaries were characterized as opaque or transparent, while gases were nonparticipating media.
- 2-D heat conduction in walls and convection heat losses from system boundaries.
- Temperature variations of density, viscosity, specific heat, thermal conductivity and diffusivity.
- Multicomponent diffusion with thermo-diffusion and species conservation. These simulations yielded temperature, enthalpy, velocity, species mass fraction and species flux at every point in the reactor, surface species mass fraction and flux at all catalytic surfaces, and heat and mass flux at every surface and boundary in the reactor.

Boundary and initial conditions

Inlet velocities, temperatures, pressures, gas compositions, and radiative properties were specified as boundary conditions. The outlets were at fixed pressure, and estimates of temperature and gas composition were specified at these outlets as boundary conditions. For the internal walls, radiative properties and surface chemistry mechanisms were specified, whereas for the external boundaries, heat transfer from the walls and radiative properties were specified. Velocity, pressure, temperature, and gas composition at every point in the reactor were specified as initial conditions. Initial surface coverages on the catalytic walls were also specified, and these were estimated by trial and error using CHEMKIN.

For the results presented in Figure 7, the initial temperature at every point in the reactor was set to 700°C to simulate light-off.

Results

Figure 7 shows simulated temperatures and CH_4 and CO mass fractions in a two-pass, 3-channel co-current system using 12,870 grid points in the reactor. As seen from Figure 7a, the temperature in the upstream section is high and falls in the downstream section as observed experimentally. High CH_4 conversions ($>$95%) are predicted for both the exothermic and endothermic sides (Figure 7b). Figure 7c shows that CO is formed in the upstream section due to steam reforming at the high temperatures and consumed in the downstream section due to water-gas shift at the lower temperatures. These all agree qualitatively with our experimental results.

The endothermic CH_4 conversion and selectivity to CO predicted for these conditions were 99.6% and 70%, respec-

tively, whereas they were experimentally observed to be 99.4% and 43%. These differences between simulation and experimental results are due to differences between predicted and observed temperatures. Also, methane steam reforming and water-gas shift kinetics on rhodium are not well known, and this contributes to differences as well.

When a good agreement between experiments and predictions is reached, these simulations will be used as a predictive tool for designing better reactors for hydrogen production.

Discussion

We discuss the role of mass transfer in the system, as well as scale-up, scale down, and transient characteristics of the reactor. Methods to increase the extent of the water-gas shift reaction are also considered.

Mass transfer

Combustion and reforming reaction rates are high at these operating temperatures, and mass transfer of methane (the limiting species) to the catalytic surface limits conversion. A simple dimensional calculation can be performed to estimate the diffusion time to the catalyst walls. For flow in the endothermic channel with reaction on two walls, the time for diffusion t to the reactive walls in laminar flow can be approximated as

$$t \cong \frac{(x/2)^2}{D} \cong \frac{(0.4\,\text{cm}/2)^2}{1\,\text{cm}^2/\text{s}} = 0.04\ \text{s}$$

where x is the gap width (4 mm) and D is an approximate gas-phase diffusion coefficient (estimated to be $\sim 1\ \text{cm}^2/\text{s}$ at the experimental temperature). The time for diffusion to the wall is only ~ 0.01 s if a plate coated with catalyst on both sides is inserted in the endothermic channel because the diffusion distance is halved. For flow in the exothermic channel with reaction on one wall, this expression predicts $t \cong 0.16$ s. Thus, the time for diffusion of the reactants to the catalyst surface is comparable to or shorter than the experimental residence time, which ensures that all the feed gases contact the catalytic surface. This also implies that reducing the gap width to 2 mm would potentially increase throughput by four times, and a 1 mm gap would increase throughput by a factor of 16.

Thermal efficiency

The thermal efficiency of these systems was calculated as the sum of the endothermic reaction heat required, which was obtained from the endothermic CH_4 conversion, and the sensible heat absorbed by the exothermic and endothermic products, divided by the exothermic reaction heat released, which was obtained from the exothermic CH_4 conversion. We calculated that ~ 40–45% of the heat generated in these systems was lost to the surroundings by conduction and radiation. These losses would be significantly lowered by adding more reaction channels to the system to reduce top and bottom losses. This would also raise temperatures in the reactor, which would permit lower CH_4 flows or leaner CH_4-air mixtures on the exothermic side.

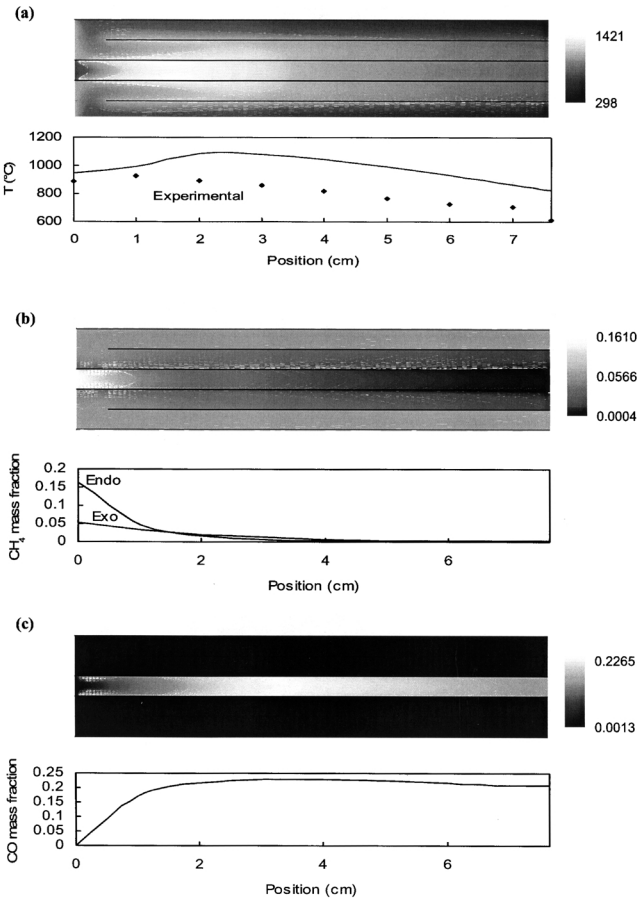

Figure 7. Simulated results of a two-pass three-channel system.

The flow rates of the exothermic gases were 0.3 slpm CH_4 and 3 slpm air, and they entered the reactor at 25°C and 1.3 atm. The flow rates of the endothermic gases were 0.2 slpm CH_4 and 0.2 slpm N_2 with a S/C ratio of 3/1, and they entered the reactor at 600°C and 1 atm. (a) Predicted temperature profile (scale in K). The plot shows the temperature profile in the middle of the exothermic channel. The closed symbols represent the experimental temperature profile. (b) Predicted CH_4 mass fraction profile. The plot shows CH_4 mass fraction profiles in the middle of the exothermic and endothermic channels. (c) Predicted CO mass fraction profile. The plot shows the CO mass fraction profile in the middle of the endothermic channel.

Scale-up and scale down

These reactors can be scaled up simply by increasing plate size and adding more channels, although it would be necessary to devise strategies to maintain desired temperature profiles in the scaled up reactors which would run closer to adiabatic conditions. Scaling down by decreasing the plate size would lead to increased heat losses, and better insulation, such as a vacuum jacket around the steam reforming zone, would be needed. The extended two-pass configuration yielded enough hydrogen to power an 80 W fuel cell, and we calculate that a similar 1 m^3 system would power a 900 kW fuel cell.

Startup and response times

By using an electrical spark to ignite the exothermic reaction, fast startup times are possible (Leclerc et al., 2002).

Heating rates of $\sim 50°C/s$ are possible for a 4 gm fecralloy plate based on the total combustion of 0.15 slpm CH_4. By starting the exothermic flows to heat the reactor before turning on the endothermic flows, startup times of < 10 s should be obtainable. These reactors also have fast response times to changes in exothermic or endothermic flows, because the heat-transfer resistance due to conduction in the thin metal wall is low, resulting in close coupling between temperatures on both sides of the wall (Figure 7a).

Water-gas shift

The water-gas shift reaction is slightly exothermic, so low temperatures favor low CO selectivities (Figure 5), whereas high temperatures are needed for fast kinetics. Optimally, operating at a relatively high temperature when the gas composition is far from equilibrium, and then lowering the temperature as equilibrium dictates conversion, maximizes the rate of CO conversion at each point along the length of the reactor (Zalc and Lóffler, 2002). Further investigations of kinetics on particular catalysts and mass-transfer rates to the catalyst surfaces are needed for designing reactors with optimal temperature drops.

The exit gas composition in the extended two-pass system at the exit temperatures was far from equilibrium, which predicts a CO selectivity of $< 1\%$ at a S/C ratio of 4/1. Since the rate of water-gas shift on noble metal-ceria catalysts is low at these temperatures (Bunluesin et al., 1998; Trovarelli, 2002), increasing catalytic surface area in the extended region might help in increasing H_2/CO ratios.

Negligible differences in the endothermic CH_4 conversions between the two-pass and the extended two-pass configurations suggest that the extent of methanation, which is the reverse of the steam reforming reaction, was low in the extended two-pass reactor where considerable water-gas shift occurred. Water-gas shift studies on various noble-metal ceria catalysts at millisecond residence times (Wheeler and Schmidt, 2002) have shown that platinum-ceria shows the lowest extent of methanation.

Summary

Catalytic wall reactors have promise as small autothermal systems to generate chemicals without external heat generation. In this work, we have demonstrated that:

(1) The system operates stably at 800 to 1,000°C for long hours without deactivation, indicating that both the catalyst and the metal walls are stable.

(2) Conversions of fuel are high: 90% or greater on the combustion side and 90 to 99% on the reforming side. Residence times required appear to be controlled by mass-transfer rates to the catalyst walls.

(3) Water-gas shift can be accomplished in the reactor at short times. We obtain $H_2/CO = 14/1$ by using rhodium in the two-pass system.

(4) With an extended two-pass system, $H_2/CO = 42/1$ can be obtained by using platinum-ceria in the extended region. This gives 45% H_2 and 1.1% CO by volume in the exit stream. This composition is suitable for selective CO oxidation and subsequent use in a PEM fuel cell.

(5) This experimental system generates sufficient H_2 for an 80 W fuel cell. It should be possible to scale the reactor up or down by at least a factor of 5 for larger or smaller applications.

(6) Using multiple channels (Figure 1b), heat losses should be reduced to obtain essentially adiabatic operation. Optimal temperature profiles should be obtainable by suitable configurations of flows and insulation.

Literature Cited

Bunluesin, T., R. J. Gorte, and G. W. Graham, "Studies of the Water-Gas-Shift Reaction on Ceria-Supported Pt, Pd, and Rh: Implications for Oxygen-Storage Properties," *Appl. Catalysis B: Environmental*, **15**, 107 (1998).

Deutschmann, O., L. I. Maier, U. Riedel, A. H. Stroemman, and R. W. Dibble, "Hydrogen Assisted Catalytic Combustion of Methane on Platinum," *Catalysis Today*, **59**, 141 (2000).

Frauhammer, J., G. Eigenberger, L. v. Hippel, and D. Arntz, "A New Reactor Concept for Endothermic High-Temperature Reactions," *Chem. Eng. Sci.*, **54**, 3661 (1999).

Igarashi, A., C. Fukuhara, S. Takeshita, C. Nishino, and M. Hanawa, "Apparatus and Method for Preparing Reformed Gas by Means of Electroless Plating," U.S. Patent No. 5,167,865 (1992).

Klein, E., and L. D. Schmidt, personal communication (2002).

Koga, M., and T. Watanabe, "Plate Type Reformer," U.S. Patent #5,015,444 (1991).

Leclerc, C. A., J. M. Redenius, and L. D. Schmidt, "Fast Lightoff of Millisecond Reactors," *Catalysis Lett*., **79**, 39 (2002).

Polman, E. A., J. M. Der Kinderen, and F. M. A. Thuis, "Novel Compact Steam Reformer for Fuel Cells with Heat Generation by Catalytic Combustion Augmented by Induction Heating," *Catalysis Today*, **47**, 347 (1999).

Redenius, J. M., L. D. Schmidt, and O. Deutschmann, "Millisecond Catalytic Wall Reactors: I. Radiant Burner," *AIChE J.*, **47**, 1177 (2001).

Trovarelli, A., *Catalysis by Ceria and Related Materials*, Imperial College Press, London (2002).

Venkataraman, K., J. M. Redenius, and L. D. Schmidt, "Millisecond Catalytic Wall Reactors: Dehydrogenation of Ethane," *Chem. Eng. Sci.*, **57**, 2335 (2002).

Wheeler, C., and L. D. Schmidt, Personal communication (2002).

Zalc, J. M. and D. G. Löffler, "Fuel Processing for PEM Fuel Cells: Transport and Kinetic Issues of System Design," *J. of Power Sources*, **111**, 58 (2002).

Manuscript received Sept. 19, 2002, and revision received Dec. 3, 2002.